Automatic Evaluation of Nickel Alloy Secondary Phases from SEM Images

Victor Hugo C. de Albuquerque[1, 2], Cleiton Carvalho Silva[3], Thiago Ivo de S. Menezes[3], Jesualdo Pereira Farias[3], João Manuel R. S. Tavares[4]

[1]Universidade de Fortaleza (UNIFOR), Centro de Ciências Tecnológicas (CCT), Núcleo de Pesquisas Tecnológicas (NPT), Av. Washington Soares, 1321, Sala NPT/CCT, CEP 60.811-905, Edson Queiroz, Fortaleza, CE, BRAZIL
Email: victor.albuquerque@fe.up.pt

[2] Universidade Federal da Paraíba (UFPB), Departamento de Engenharia Mecânica (DEM), Laboratório de Solidificação Rápida (LSR), Centro de Tecnologia - Campus I, Cidade Universitária, 58059-900 - Joao Pessoa, PB - BRAZIL

[3]Universidade Federal do Ceará (UFC), Departamento de Engenharia Metalúrgica e de Materiais (DEMM), Laboratório de Engenharia de Soldagem (ENGESOLDA), Campus do Pici, S/N – CEP 60455-760, Fortaleza, CE, BRAZIL
Emails: cleitonufc@yahoo.com.br, thiagoivo@hotmail.com, jpf@secrel.com.br

[4]Instituto de Engenharia Mecânica e Gestão Industrial (INEGI)
Faculdade de Engenharia da Universidade do Porto (FEUP), Departamento de Engenharia Mecânica (DEMec), Rua Dr. Roberto Frias s/n, 4200-465, Porto, PORTUGAL
Email: tavares@fe.up.pt

Corresponding author:
Prof. João Manuel R. S. Tavares
Instituto de Engenharia Mecânica e Gestão Industrial (INEGI)
Faculdade de Engenharia da Universidade do Porto (FEUP)
Departamento de Engenharia Mecânica (DEMec)
Rua Dr. Roberto Frias s/n
4200-465 PORTO
PORTUGAL
Phone: +315 22 5081487, Fax: +315 22 5081445
Email: tavares@fe.up.pt Url: www.fe.up.pt/~tavares

Automatic Evaluation of Nickel Alloy Secondary Phases from SEM Images

Abstract

Quantitative metallography is a technique to determine and correlate the microstructures of materials with their properties and behavior. Generic commercial image processing and analysis software packages have been used to quantify material phases from metallographic images. However, these all-purpose solutions also have some drawbacks, particularly when applied to segmentation of material phases. To overcome such limitations, this work presents a new solution to automatically segment and quantify material phases from SEM metallographic images. The solution is based on a neuronal network and in this work was used to identify the secondary phase precipitated in the gamma matrix of a Nickel base alloy. The results obtained by the new solution were validated by visual inspection and compared with the ones obtained by a commonly used commercial software. The conclusion is that the new solution is precise, reliable and more accurate and faster than the commercial software.

Keywords: Materials Sciences; Metallography; Microstructural Analysis; Nickel Alloy; Secondary Phase; Precipitation; Phase Quantification; Dissimilar Metal Weld; Image Segmentation; Artificial Neuronal Network.

1 Introduction

Nickel (Ni) base alloys belong to one of the most important classes of corrosion-resistant materials that are used in overlay applications (Lievers and Pilkey, 2004). During the weld solidification of these alloys, intense microsegregation of some elements, such as molybdenum (Mo), niobium (Nb), titanium (Ti) and tungsten (W), into interdendritic regions causes supersaturation of the material in its final stage of solidification, which causes the formation of secondary phases such as P, σ, μ (Cieslak et al., 1986), laves and carbides (Dupont, 1996). These secondary phases can change the mechanical properties of the material and decrease its resistance to corrosion (Yang et al., 2006). For example, in the Inconel 625 alloy the secondary phases in as-welded condition are MC carbides of the (NbTi)C type and Nb-rich Laves phase (Cieslak, 1991). Ni-based alloys are very susceptible to hot cracking due to Nb-rich Laves phase formation that has a low melting point (Dupont et al., 2003). Thus, it is very important to quantify the phase precipitates so that the most suitable welding parameters that minimize the presence of these particles, can be selected. In order to determine the percentage of secondary phases, all-purpose image processing and analysis software packages are frequently used (Pan et al., 2005).

Many computational solutions to segment and quantify material microstructures from images have been developed. Generally, most of the commercial solutions, for microstructural characterization from images, are based on the traditional threshold method to segment the input images. On the other hand, various computational systems have been developed to evaluate material microstructures from images that are based on more efficient segmentation techniques. For example, Albuquerque et al. (2008) presents a comparative analysis between a commercial tool and a custom built backpropagation neuronal network for the identification and quantification of material microstructures from metallographic images. In their work,

Albuquerque et al. showed that the neuronal approach was more efficient, reliable and accurate. To evaluate the segmentation quality and the quantification effectiveness, Albuquerque et al. (2009) tested two neuronal topologies, a multilayer perceptron and a self-organizing map, on metallographic images of cast iron samples. From their experimental findings, the multilayer perceptron neuronal network was shown to be more accurate and more efficient. However, these enhanced computational systems have been developed to perform the analysis of material microstructures from images and not specifically designed for the study of the secondary phase of Ni-base alloys, leading to rather inefficient solutions. This limitation of the present computational systems has been overcome by the new solution described in the following sections. Additionally, it is important to stress that, as far as the authors know, there are no studies in the current literature about the efficiency of segmentation and quantification of Ni-base alloys under the welding conditions used in this work, making the results of this work to be of some consequence.

2 Experimental procedure

The main goal of this work is the development and evaluation of a new computational solution, based on an artificial neuronal network, to automatically and efficiently quantify the secondary phases of Ni-base alloys from SEM images. The results obtained by the new solution were assessed by visual inspection and compared with the ones from a commercial image processing and analysis software package that is frequently used in microstructural evaluation of materials from images. The evaluation of the new solution took into account: segmentation quality and accuracy; reliability of the results obtained and time. In this section, the experimental procedure is detailed.

Samples extracted from Inconel 625 alloy coatings deposited by welding on an ASTM (American Society for Testing and Materials) A516-Gr 60 steel substrate were used in the experimental work. The chemical composition of the weld metal is shown in Table 1. The test samples were extracted from the welded plates and subsequently underwent a metallographic preparation that included sanding, polishing and electrolytic attack, using 10% chromic acid with a 2V tension for 15 seconds.

An initial attempt was made to obtain the images for the experimental evaluation by light microscopy, due to its simplicity when compared to other microscopic techniques. However, although the metallographic preparation of the testing samples was adequate, the images did not show a satisfactory distinction between the precipitates involved and the matrix, Figure 1. Consequently, scanning electron microscopy was used.

The images were acquired using a Phillips FEG XL30 scanning electron microscope (USA). In the backscattering electron (BSE) operation mode it is possible to select the imaging contrast by atomic weight (Z-contrast) (Korcakova et al., 2001). However, the images in the SE (secondary electron) mode offered a superior contrast between the precipitates and the matrix, probably due to the enriched precipitates with higher atomic weight elements, such as Mo, Ti and Nb.

Therefore, after adequate preparation of the test samples, the images were obtained by SEM in the SE mode on a 1000x scale and were then analyzed by the two computational solutions for comparison and also by two specialists in metallographic image analysis.

To analyze the SEM images two computational solutions were used. One was an all-purpose commercial image processing and analysis software, frequently used for microstructural

evaluation and the other was the new solution developed here, which was based on a multilayer neuronal network.

In the image segmentation step, the commercial software uses the traditional global threshold technique. The numeric value for the threshold has to be defined by the user for the image to be analyzed and this consequently introduces the possibility of segmentation errors, mainly when the input image contains noise and other artifacts. Additionally, this manual procedure is highly subjective and with low reproducibility. The new solution overcomes such limitations, without imposing high computational complexities that are required by other image segmentation methods such as the watershed or level set methods, by using an artificial neuronal network. (For a review on image segmentation methods, see, for example, (Ma et al., 2010).)

The backpropagation training algorithm is used for the training of the new solution network. In this training, the user just needs to define the phases to be segmented and quantified, by indicating a set of sample pixels for each phase from one or more representative images. After the training, the user only needs to place the images for the new solution and the analysis is fully automatic. As far as the authors know, the proposed solution is the first to evaluate the microstructure of Ni-Base alloy secondary phases from SEM images, which presents low computational complexity, high efficiency, considerable accuracy, reliability and reproducibility.

2.1 Artificial Neuronal Networks

A human brain is composed of around ten billion neurons and their organization is of high structural and functional complexity. These neuron units are densely interconnected, which results in a very complex architecture and with an intelligence level that has not yet been achieved by any system developed by man. Several numerical models have been developed to

simulate neurons and their interconnection, like artificial neuronal networks, in an attempt to reproduce human brain potentialities, especially its learning ability (Haykin, 2009).

McCulloch and Pitts (McCulloch and Pitts, 1943) proposed the first mathematical neuron model. It had a binary output and several inputs, each one with a different excitatory or inhibitory gain. These gains are known as synaptic weights or simply as weights.

Fundamentally, an artificial neuron, that is, a perceptron, is the mathematical model of a neuron cell and the basic unit that makes up an artificial neuronal network (ANN). Perceptron architecture consists of a set of inputs, each one associated to a synaptic weight and an activation function. All neurons of the input layer are fully interconnected to all neurons of a hidden layer that are fully interconnected to all neurons of the output layer, making up a network that is designated as a perceptron network. However, perceptron networks only achieve good performances when the modeled system is linearly separable (Haykin, 2009). Therefore, perceptron networks should not be used to solve complex classification problems involving non-linearly separable problems, in which multilayer perceptron networks should be employed. In this case, the input signal values are correlated with the network outputs through the correct adjustment of the neuron synaptic weights until the desired solution is outputted. This adjustment process can be performed off-line and then the ANN is supervised, as the one used in the new solution, or can be performed in-runtime, in which case the ANN is not supervised (Haykin, 2009).

The backpropagation multilayer perceptron learning algorithm was developed in the early 1970's by several researchers (Singh and Rao, 2005). This extensive development resulted in a wide dissemination of perceptron networks, which also stimulated their industrial use. Currently, the backpropagation algorithm is the most common and most effective network, and it is easy to

build complex models for multilayered neuronal networks. Mainly due to its accuracy and high speed it has been widely used (Werbos, 1974).

One of the most common backpropagation network topologies has an input layer, an output layer and, at least, one hidden layer. There is no theoretical limitation to the number of hidden layers, but typically there is just one, the most usual case, or two hidden layers (Alsmadi et al., 2009).

2.1.1 Architecture of the neuronal network used

As previously stated, the main aim of this new computational solution was to evaluate the microstructure of the secondary phases of Ni-base alloys from SEM images using a multilayer perception neuronal network in the image segmentation step. Thus, in this step, each pixel of the input image is classified according to the secondary phase to which it belongs.

The new solution adopted multilayer perceptron architecture for the neuronal network and the backpropagation algorithm to train it. The network topology was defined as: an input layer composed of 3 neurons; one hidden layer composed of 7 neurons, this number was defined by adopting the heuristic rule proposed by Kolmogorov (Bodyanskiy et al., 2005), in which the number of neurons in the hidden layer is twice the number of neurons in the input layer plus 1 (one); and finally, 3 neurons in the output layer that is related to the number of possible classifications. Figure 2 shows the 3/7/3 topology of the neuronal network used. The logistic function (Elliott and Better, 1993, 1993) was used as the activation function, which has three possible output values: 1 (one), 0 (zero) and -1 (one).

The SEM images used were grayscale images. However, the neuronal network used had 3 inputs, and so it could also be employed in the segmentation of color images. Thus, when applied

in color images, the red, green and blue components of each image pixel are presented to the corresponding input neuron of the network and when applied to grayscale images the value of each image pixel is presented to an input neuron of the network and the other two are unused. Moreover, as the network has 3 outputs and the logistic function was used as the activation function up to 27 classes could be classified.

The process of training a neuronal backpropagation network consists of two steps:
The first step is characterized by the forward direction. It first considers the neuronal network input values, and then it calculates the activations and outputs of all neurons in the hidden layer and in the output layer. Therefore, the flow of input values in the network starts in the input layer neurons, goes through the knots in the hidden layer, and finally, to the neurons in the output layer, where the network result is obtained.

Thus, after the definition of the network input value, x, in this case corresponding to the image value of each pixel selected for the training, the activations of the neurons in the hidden layer are calculated as:

$$u_i(t) = \sum_{j=0}^{p} w_{ij}(t) x_j(t), \text{ with } i = 1,...,q, \tag{1}$$

where q indicates the number of neurons in the hidden layer. Finally, the outputs that correspond to these neurons are calculated as:

$$z_i(t) = \phi_i(u_i(t)) = \phi_i(\sum_{j=0}^{p} w_{ij}(t) x_j(t)), \tag{2}$$

where ϕ_i corresponds to the activation function of the hidden layer. Here, the logistic function, also called sigmoid function, a continuous function that allows the gradual transition between states was adopted as the activation function and is given as:

$$\phi_i(u_i(t)) = \frac{1}{1+\exp[-u_i(t)]}. \quad (3)$$

The next phase repeats the operations associated to equations (1) and (2) for the output layer neurons:

$$u_k(t) = \sum_{i=0}^{q} m_{ki}(t) z_i(t), \text{ with k} = 1,...,M, \quad (4)$$

where M is the number of neurons in the output layer. As would be expected, in these equations the outputs of the hidden layer neurons, $z_i(t)$, correspond to the inputs of the output layer neurons. Finally, the classification obtained from the neurons in the output layer is:

$$y_k(t) = \phi_k(u_k(t)) = \phi_k(\sum_{i=0}^{q} m_{ki}(t) z_i(t)), \quad (5)$$

where ϕ_k is the activation function of the output layer that was considered to be the logistic function.

In the second step of the neuronal backpropagation network training, the feedback information is transferred through the network in a reverse direction and calculates the local gradients and the adjustment of synaptic weights of all neurons in the hidden and output layers. However, in this step, if the neural network does not provide the output expected, the data flows through the network from the neurons in the output layer to the neurons in the hidden layer.

After the calculation of activations and outputs performed in the previous step, the first phase in this second step calculates the local gradients of the output layer neurons:

$$\delta_k(t) = e_k(t)\phi'(u_k(t)), k = 1,...,M, \quad (6)$$

where $e_k(t)$ corresponds to the error, $e_k(t)$, obtained between the desired output, $d_k(t)$, for the neuron k and the associated output generated, $o_k(t)$, given as:

$$e_k(t) = d_k(t) - o_k(t) \quad (7)$$

Considering once again the logistic function as the activation function of the neurons in the hidden and output layers, one obtains:

$$\phi'(u_k(t)) = \frac{d\phi_k(u_k(t)}{du_k(t)} = y_k(t)[1 - y_k(t)]. \quad (8)$$

The second phase of this step calculates the local gradients of the hidden layer neurons:

$$\delta_i(t) = \phi'_i(u_i(t)) \sum_{k=1}^{n} m_{ki}\delta_k(t), \text{ with } i = 1,...,q, \quad (9)$$

where the $\phi'(u_i(t))$ is calculated as:

$$\phi'(u_i(t)) = \frac{d\phi_i(u_i(t)}{du_i(t)} = y_i(t)[1 - y_i(t)]. \quad (10)$$

Then, the third phase updates or adjusts the network synaptic weights. Thus, the weight updating, w_{ij}, for the hidden layer is given by:

$$w_{ij}(t+1) = w_{ij}(t) + \Delta w_{ij}(t) = w_{ij}(t) + \alpha\delta_i(t)x_j(t), \quad (11)$$

where $\alpha(t)$ corresponds to the learning rate, considered as equal to 0.1 in the implementation of the new solution. For the output layer, the updating rule of synaptic weights, m_{ki}, is:

$$m_{ki}(t+1) = m_{ki}(t) + \Delta m_{ki}(t) = m_{ki}(t) + \alpha\delta_k(t)z_i(t). \quad (12)$$

The criteria adopted to stop the training of the neuronal network used are an absolute error equal or inferior to 0.01 or a number of iterations equal to 2,500.

In the developed solution, the neuronal network is trained from a given set of SEM images representing the material understudy and the values of these image pixels that are representative of each material phase to be segmented by the network. According to the quality of the segmentation results, a new adjustment of the network synaptic weights may be necessary, that is, to obtain better results, the network is retrained by using more or better training images and/or image pixels.

From a total set of 72 images acquired by SEM, 18 randomly chosen images were used to train the neuronal network. From each image 12 pixels were selected and averaged for each of the two phases to be segmented. The remaining 54 images were then analyzed by the new solution and by the commercial system and the results evaluated.

Initially, the comparison of the two computational solutions was based on the quality of the segmentations obtained. Thus, various image segmentations were carried out in order to reach a 95% reliability level, considering statistical analyses like mean, standard deviation and relative error. Additionally, the times required to study each input image were analyzed as well as the total times to study a set of 20 images randomly chosen from the 54 test images.

3 Experimental Results and Discussion

First, the testing samples were metallographically prepared by mechanical sanding and polishing using diamond paste as abrasive. To reveal the microstructure of the Ni-base alloy welding metal, a chemical etching with an aqueous solution containing 10% of chromic acid was carried out. The etching clearly revealed the material matrix and secondary phases precipitated at the end of alloy solidification. Then, 72 SEM images were acquired with a 640 x 480 resolution.

The commercial system, adopted here just for purposes of comparison and validation, required the following steps: load the image; transform the original image into an 8-bit image; segment the converted image using the traditional threshold method, by manually selecting the threshold; quantify the segmented regions. On the other hand, the new computational solution, after the training of the neuronal network as described above, only required these steps: load the image; segment the original image and obtain the quantification results automatically.

As mentioned in the previous section, the SEM images were obtained in the SE mode, giving a contrast level suitable for a reasonable differentiation between the material precipitates and phases. Therefore, the material samples, which had sufficient metallographic quality and the good SEM images acquired from them, could be successfully processed by both the computational solutions under evaluation. Figure 3a shows one of the images that was easily and successfully segmented by both computational solutions, as the precipitates and phases are satisfactory defined and distinguished. Both the segmentations carried out were adequate and similar, Figure 3b and 3c.

However, occasionally, neither computational solution was able to identify some of the smaller or poorly defined precipitates with accuracy. Nevertheless, to improve the quality of the segmentation of the new solution was very simple and immediate: to obtain good segmentation results from these lower quality images, it was only necessary to perform a new network training to obtain a better adjustment of the synaptic weights. On the other hand, the attempt to improve the segmentation of the same images with the commercial solution revealed to be troublesome or even impossible. This is because the threshold method is based upon the histogram obtained from the input image and the threshold level to be used is manually selected, which is very complicated from low quality images. In addition, since it is a global segmentation method, it

frequently leads to improved results in certain areas but worse results in others. This problem is illustrated in Figure 4, considering the area detached from the original image, Figure 4a, which is magnified in Figure 4b, one can see that the image presents precipitates with a high glow and the matrix (center of the dendrite). These precipitates have a dark gray tone and also structures in light gray that correspond to the interdendritic region, which are not the precipitates of interest and can lead to erroneous results. Figure 4c shows that the segmentation by the commercial system was incorrect as the interdendritic region (matrix) is incorporated in the segmented precipitates. However, Figure 4d shows a correct segmentation of the same image by the new solution.

Using the new solution with its neuronal network trained with other SEM images with good quality and adequate contrast between matrix and precipitates, the segmentation of such images were successfully carried out. Then, the proposed solution was employed on a new test image that presented a distinct contrast between matrix and precipitates in comparison with the images used in the network training, Figure 5a. Now as can be seen in Figure 5b, the new solution erroneously considered part of the matrix that presented a light gray level as precipitate particles, resulting in an unreliable segmentation. However, this problem was once more successfully solved by retraining the neuronal network from the image to be analyzed, Figure 5c. This shows the versatility of the new solution. It should be pointed out that the use of the commercial system on these images of reduced quality and high complexity never led to correct segmentations, as it always considered part of the matrix as precipitates.

In the training phase of the neuronal network employed in the new solution, only the values of sample pixels of each material phase to be analyzed were considered. To evaluate the influence of the number of sample pixels used on the segmentation results in terms of accuracy

and speed, 20 images were randomly selected from the original set of 72 SEM images. From these 20 images, 14 images were randomly used in the training and the other 6 images were used in the evaluation. In the first evaluation only 6 training pixels of the precipitates and matrix regions were selected and the solution failed in the segmentation of 3 test images. However, after a correct adjustment of the network synaptic weights through the selection of new and more adequate training pixels, the solution could accurately segment all test images. The total time for the analysis of the 6 test images was 168 seconds. In the second evaluation, 9 pixels of each region understudy were used instead and all segmentations were adequate for all 6 testing images and the total time was reduced to 140 seconds. In the third evaluation, 12 pixels of each region understudy were used and the same segmentations were obtained with a reduction in the required time to 112 seconds. Finally, in the fourth and last evaluation, 15 pixels of each phase to be segmented were used, and the same segmentation results were obtained in a total time of 109 seconds. Thus, based on these evaluations, for further studies, 12 training pixels for each material phase were used. This option presented accurate results and low computational cost, Figure 6.

In some images acquired by SEM, it was noted that the associated samples were chemically attacked more than necessary or that the glow and contrast used were not adequate. As an example, Figure 7a shows one of these images in which the material was excessively attacked. Assessing the original image (Figure 7a), it is possible to observe glowing regions along the borders of the interdendritic regions. This increased glow brings the tone of this region closer to the precipitate tone. Figure 7b shows the pixels considered in the training phase of the neuronal network employed in the new solution to segment this image. Figure 7c, shows the resultant segmented image that shows three distinct regions: dendrite core in green, interdendritic region in yellow and particle precipitates in blue. From these images, one can conclude that when

the image pixels corresponding to the precipitates are analyzed by the neuronal network, it interprets them as being secondary phases due to the similarities in terms of tone between precipitates and matrix. As a result, the image is wrongly segmented, Figure 7c. This figure shows the presence of segmented dots in blue along the interface between the green region (core) and the yellow region (interdendritic) and blue dots also along the center of the yellow region. In fact, there is excessive segmentation of the glowing regions of the matrix, causing an erroneous increase in the quantity of precipitates. Obviously, the best solution in these cases is to repeat the metallographic preparation of the sample by submitting them to a new chemical attack with lower exposure times. Accordingly, Figure 8a shows the SEM image of a reprocessed sample, which was successfully segmented by the new solution. This image has three regions that are clearly distinct: dendrite center in dark gray, interdendritic region in light gray and glowing dots that constitute the secondary phases precipitated during the material solidification. As shown by Figure 8b, this image was successfully segmented by the new solution.

To illustrate another usual problem related to the incorrect adjustment of contrast and glow during the acquisition of the SEM images, which were effectively overcome by the proposed solution. Figure 9a shows an image that was only partially segmented successfully by the proposed solution, previously trained using images very distinct from this one. However, after retraining the neuronal network using adequate sample pixels, the images were correctly segmented, Figure 9b.

At this time, it is important to emphasize that in the cases of the images shown in Figures 8 and 9, the commercial system was not applied, since the threshold level used in the segmentation is manually defined in function of the input image, making the results totally dependent on the operator's subjectivity.

The second part of the comparison between the two computational solutions was based on their efficiency in terms of the time required to fully analysis 20 images randomly selected. Table 2 shows the times needed to carry out the segmentation and the subsequent quantification of each one of these 20 images. This table shows that the average time to perform a quantification using the new solution was approximately 9 seconds, while the commercial system had an average time of around 20 seconds. This is almost a 55% reduction in the average time required to analyze a SEM image by the proposed solution when compared to the commercial system.

The commercial solution, besides being more time consuming, requires higher user intervention. The user must be experienced and he/she needs to define the threshold level for each input image. This manual definition of the threshold value is tiring and frequently leads to errors. The new computational solution, on the other hand, significantly reduces the analytic time. Furthermore, the new solution minimizes user intervention, as it always segments images that are compatible to the ones used in the network training, correctly and automatically.

After recording the required time to analyze each image by both computational solutions, the total time required to segment and subsequently quantify a batch of 20 images of the same type was taken. For the new solution, about 5 minutes and 20 seconds were required, including the time needed to train the neuronal network. The commercial software required approximately 8 minutes and 50 seconds to do the same work. Thus, the new solution presents a reduction of 40% in the required time when compared to the commercial system.

Another factor that was analyzed and compared was the influence of user experience in handling the two computational solutions. The total time that three users, specialists in metallographic analysis and without previous contact with the solutions under evaluation, needed to analyze a group of 20 test images was recorded, Figure 10. This figure shows that the required

time to use the commercial software varied significantly, as the segmentation method employed strongly depends on user skill and attention. However, the same variation was lower when the new solution was considered, as the user influence is minimal.

Afterwards the new solution showed that with a set of 54 test images, it could achieve a reliability of 95%. While the commercial software only achieved a reliability of 34% with the same images. One can conclude that the commercial software needs around 350 test images to achieve a statistical reliability of 95%, which would result in a considerable increase of the analytic time required. This large number of test images would also impose some constraints, such as a potential tiring effect on the user due to the long analytic time. Figure 11 shows the average values as well as the standard deviations resulting from this experiment. From this Figure, a significant difference between the standard deviations from the new solution and the commercial software is clearly seen. This experiment once again emphasizes the two advantages of the new solution: higher efficiency and reliability.

Finally, given that there are no works in the current literature able to assist the evaluation of the proposed solution in terms of reliability, due to the specificity of the welding conditions that modifies the involved phase characteristics, including its quantity and geometry, 9 test images were randomly selected from the test image set and analyzed by the new solution and also by visual inspection by two specialists on microstructural analysis. In Table 3, the statistical analysis of the results obtained is presented. From this Table, one can conclude that the results obtained are very similar, proving the accuracy of the new solution. Only for illustrative purposes, Figure 12 shows one of the 9 test images, the resultant image of the visual inspection performed by one of the specialists (it should be noted that the results between the two specialists were very similar) and the resulting image by the new solution. From the results obtained, one can confirm

that the quantification made by the new solution is of superior quality as it includes small precipitate particles that were not successfully visually detected by the specialists.

To conclude, from the experimental evaluations performed, the new computational solution, which is based on an artificial neuronal network and the first custom developed system to accomplish the automatic evaluation of secondary phases of Ni-base alloys from SEM images, revealed low computational complexity, high efficiency, considerably accuracy and stableness. Its main disadvantage is the required training of the neuronal network. However, this step only needs to be carried out once for the same sort of SEM images.

4 Conclusions

Based on the quantification results of secondary phases in Ni-based alloys from SEM images using two computational solutions, one commercial software commonly used in this domain that is based on the traditional threshold method and a new solution based on a neuronal network, it was possible to conclude that the new solution is more efficient and reliable and less effected by image noise and other disturbances and also less dependent on user subjectivity. Additionally, its utilization, even by less experienced users, revealed to be easy and fast, making the analysis less tiring and therefore less likelihood of introducing errors.

With the new solution, it was possible to achieve a statistical reliability level of 95% from the 54 SEM test images, while the commercial system only presented 34%. In addition, the new solution is nearly 50% faster than the commercial software. These advantages also confirm that the new solution is a suitable option to be used in the characterization of secondary phases formed in the dissimilar welds of Ni-based alloys.

Acknowledgements

The authors are grateful for the support given by the Mechanical Testing Laboratory of the Federal Center for Technological Education in Ceará (Brazil), and to the Welding Engineering Laboratory of the Federal University of Ceará (Brazil).

The authors would like also to thank the financial support from the Brazilian research agencies: CNPq - The National Council for Scientific and Technological Development, FINEP - Research and Projects Financing and CAPES - Coordination for the Improvement of People with Higher Education.

References

Albuquerque VHC, Cortez PC, de Alexandria AR, Tavares JMRS. 2008. A new solution for automatic microstructures analysis from images based on a backpropagation artificial neuronal network. Nondestructive Testing and Evaluation 23:273-283.

Albuquerque VHC, de Alexandria AR, Cortez PC, Tavares JMRS. 2009. Evaluation of multilayer perceptron and self-organizing map neuronal network topologies applied on microstructure segmentation from metallographic images. NDT and E International 42:644-651.

Alsmadi MKS, Omar KB, Noah SA. 2009. Back propagation algorithm: the best algorithm among the multi-layer perceptron algorithm, International Journal of Computer Science and Network Security 9:378-383.

Bodyanskiy Y, Kolodyazhniy V, Otto P. 2005. Neuro-fuzzy Kolmogorov's network for time series prediction and pattern classification. Lecture Notes in Computer Science 3698:91-202.

Cieslak MJ, Headley TJ, Romig Jr AD. 1986. The welding metallurgy of HASTELLOY alloys C-4, C-22 and C-276. Metallurgical and Materials Transactions A 17A:2035-2047.

Cieslak MJ. 1991. The welding and solidification metallurgy of alloy 625. Welding Journal 70:49-56.

Dupont JN, Banovic SW, Marder AR. 2003. Microstructural evolution and weldability of dissimilar welds between a super austenitic stainless steel and nickel-based alloys. Welding Research 82:125-156.

Elliott DL, Better A. 1993. Activation Function for Artificial Neuronal Networks, ISR Technical Report TR 93-8, Institute for Systems Research, University of Maryland.

Haykin, S. 2009. Neuronal Networks and Learning Machines. Ontario, CA: McMaster University, Prentice Hall.

Korcakova L, Hald J, Somers MAJ. 2001. Quantification of Laves phase particle size in 9CrW steel. Materials Characterization 47:111-117.

Lievers WB, Pilkey AK. 2004. An evaluation of global thresholding techniques for the automatic image segmentation of automotive aluminum sheet alloys. Materials Science and Engineering A 381:134-142.

Ma Z, Tavares JMRS, Jorge RN, Mascarenhas T. 2010. A Review of Algorithms for Medical Image Segmentation and their Applications to the Female Pelvic Cavity. Computer Methods in Biomechanics and Biomedical Engineering, DOI: 10.1080/10255840903131878 (in press).

Mcculloch W, Pitts W. 1943. A logical calculus of the ideas immanent in nervous activity. Bulletin of Mathematical Biology 5:115-133.

Pan YM, Dunn DS, Cragnolino GA. 2005. Topologically close-packed phase precipitation and thermal stability in alloy 22. Metallurgical and Materials Transactions A 36:1143-1151.

Singh V, Rao SM. 2005. Application of image processing and radial basis neuronal network techniques for ore sorting and ore classification. Minerals Engineering 18:1412-1420.

Werbos PJ. 1974. Beyond regression: new tools for prediction and analysis in the behavioral sciences. Ph.D. Thesis, Harvard University.

Yang JX, Zheng Q, Sun XF, Guan HR, Hu ZQ. 2006. Formation of l phase during thermal exposure and its effect on the properties of K465 superalloy. Scripta Materialia 55:331-334.

TABLE CAPTIONS

Table 1. Chemical composition of weld metal.

Table 2. Results obtained from the two solutions under evaluation for the quantification of 20 SEM test images.

Table 3. Statistical analysis of the quantification of precipitate particles from SEM images by the new solution and by the visual inspection of two specialists.

FIGURE CAPTIONS

Figure 1. Image acquired by light microscopy.

Figure 2. Topology of the neuronal network used in the new solution.

Figure 3. a) Original SEM image, b) image segmented by the new solution and c) image segmented by the commercial software.

Figure 4. Comparison between the two computational solutions under evaluation: a) Original SEM image, b) Magnification of the detail indicated in a), c) image segmented by the commercial solution and d) image segmented by the new solution.

Figure 5. Illustration of effect of the neuronal network training: a) Image obtained by SEM; b) Segmentation performed with an initially training of the neuronal network and c) Segmentation performed after the retraining of the neuronal network.

Figure 6. Analysis on the influence of the number of pixels per phase used in the training of the neuronal network in the required segmentation time.

Figure 7. a) Image obtained by SEM with excessive chemical etching, b) pixels used in the training of the neuronal network and c) segmentation obtained using the new solution.

Figure 8. a) Image obtained by SEM with an adequate level of chemical etching and b) Segmentation obtained using the new solution.

Figure 9. a) Image obtained by SEM used in the first training of the neuronal network and b) Segmentation obtained using the new solution.

Figure 10. Comparison on the performance of three users in the segmentation of 20 SEM images using the new solution and the commercial solution.

Figure 11. Statistical analysis on results obtained by the computational solutions in the analysis of 54 SEM test images.

Figure 12. a) An original SEM image with precipitate particles, b) segmentation result by visual inspection by one specialist and c) the segmentation result by the new solution.

FIGURES

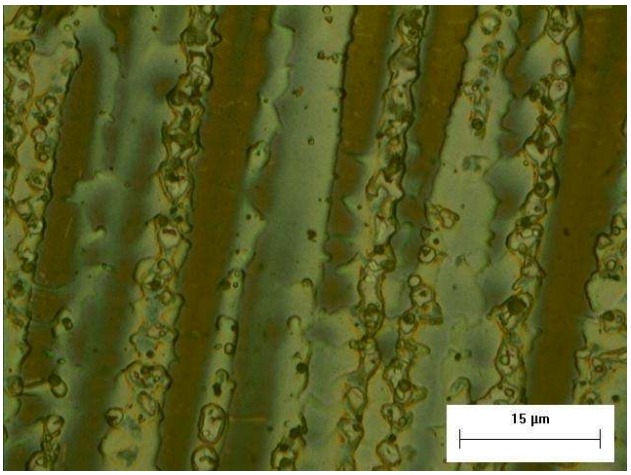

Figure 1

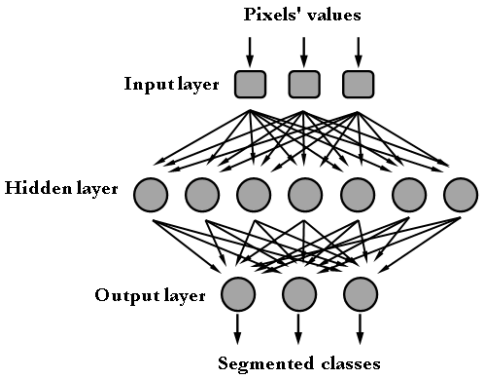

Figure 2

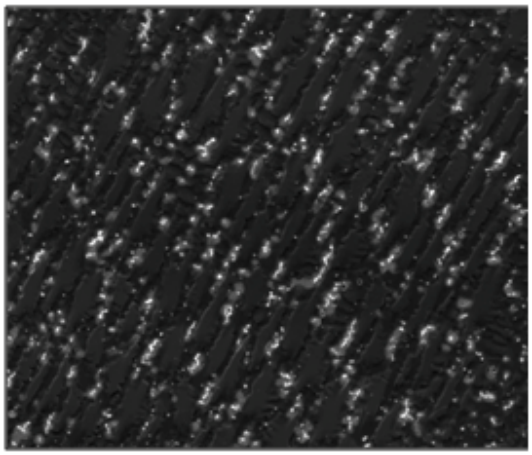

Figure 3a

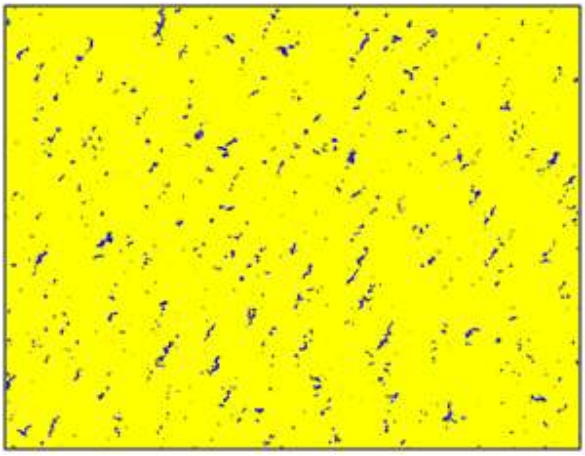

Figure 3b

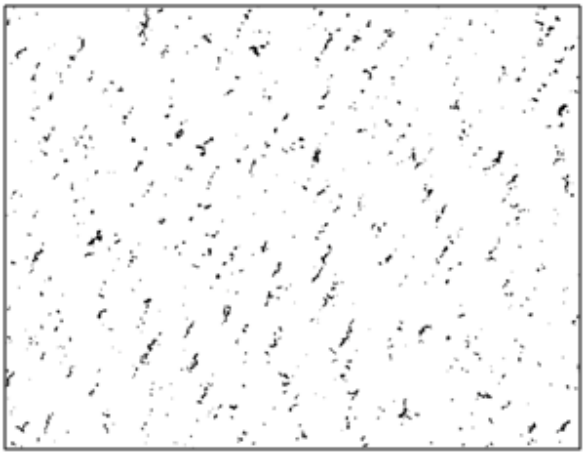

Figure 3c

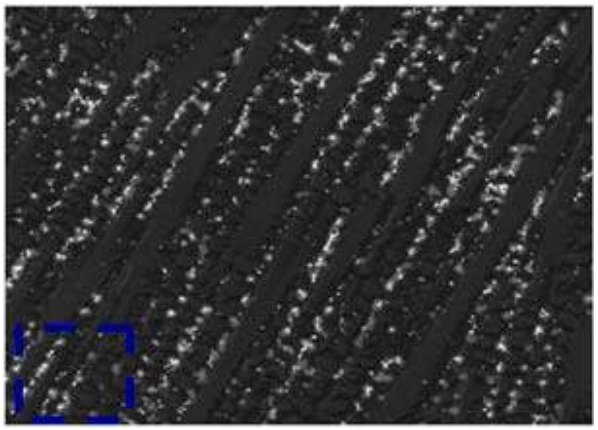

Figure 4a

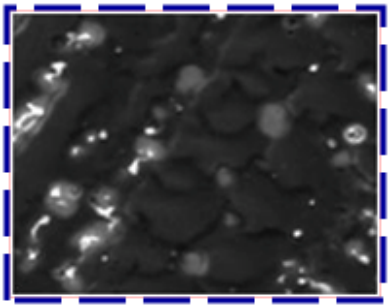

Figure 4b

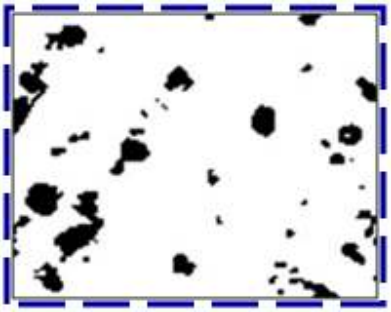

Figure 4c

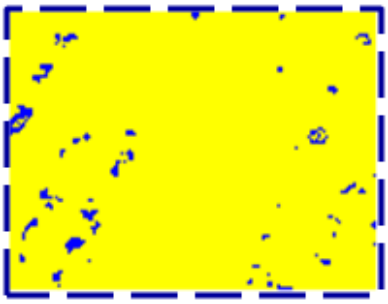

Figure 4d

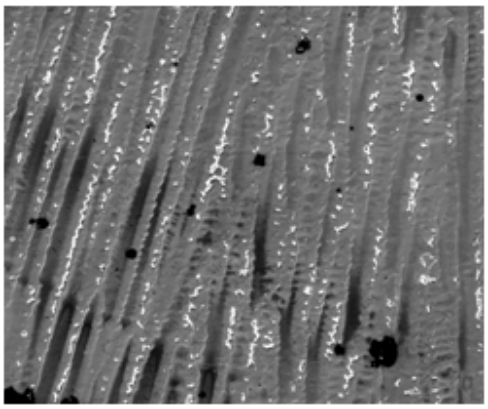

Figure 5a

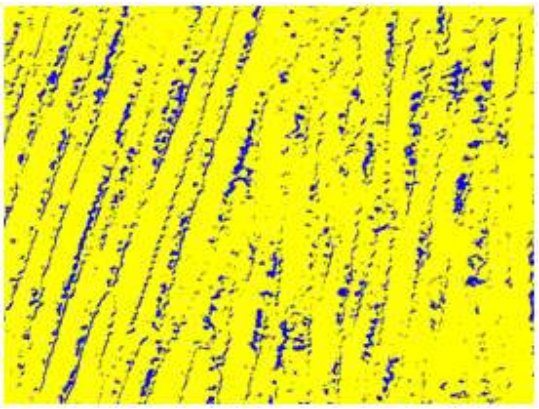

Figure 5b

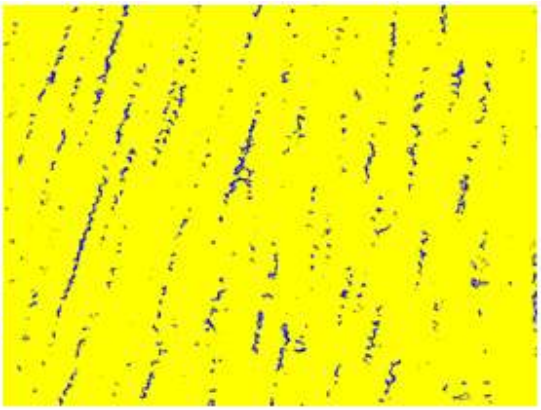

Figure 5c

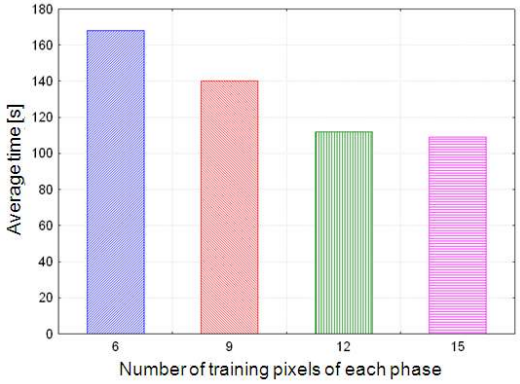

Figure 6

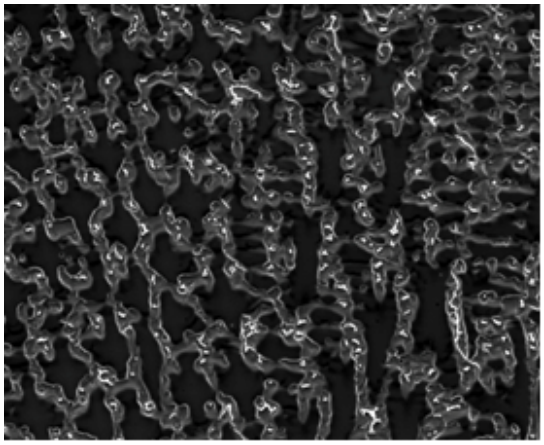

Figure 7a

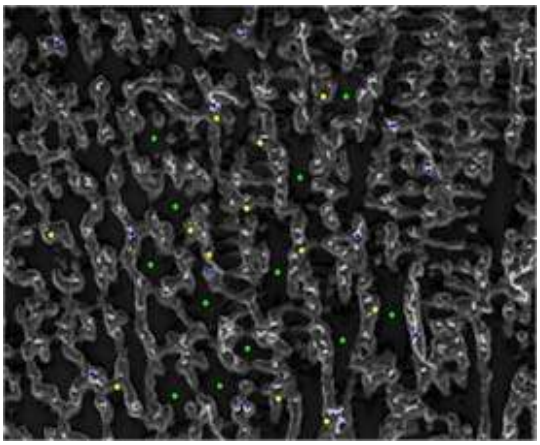

Figure 7b

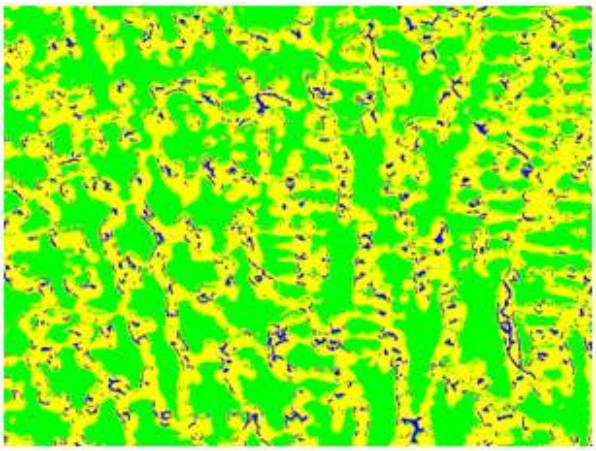

Figure 7c

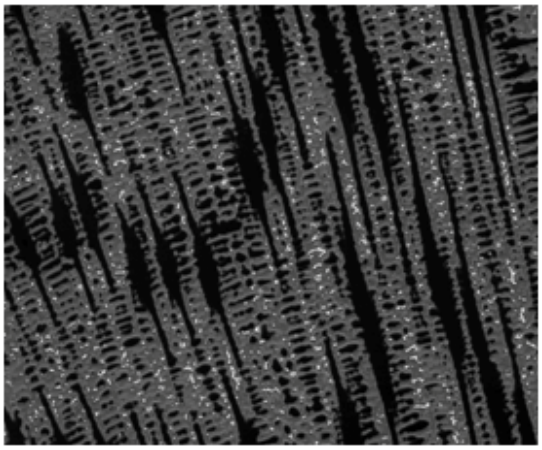

Figure 8a

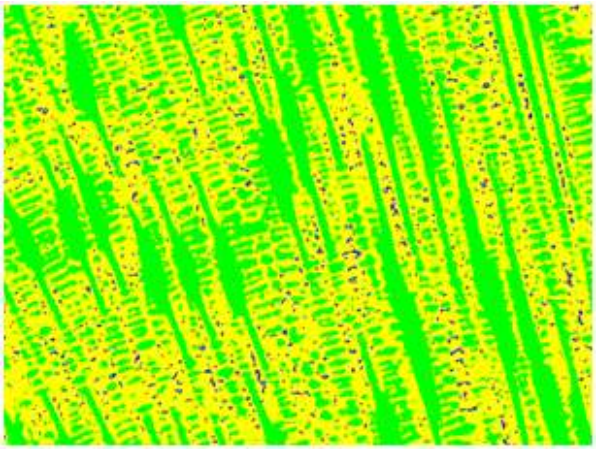

Figure 8b

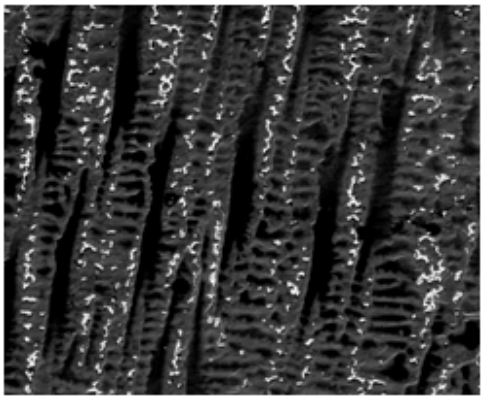

Figure 9a

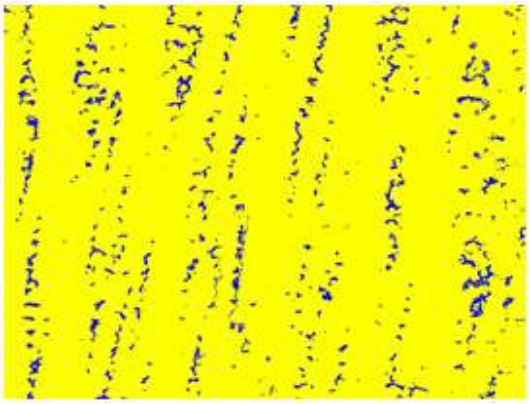

Figure 9b

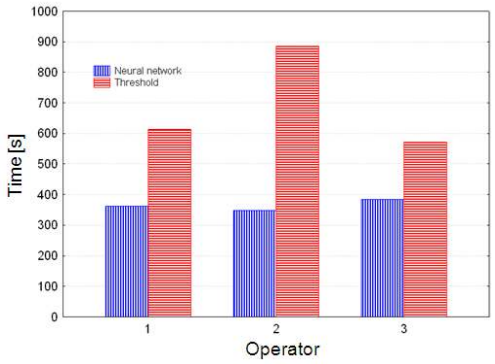

Figure 10

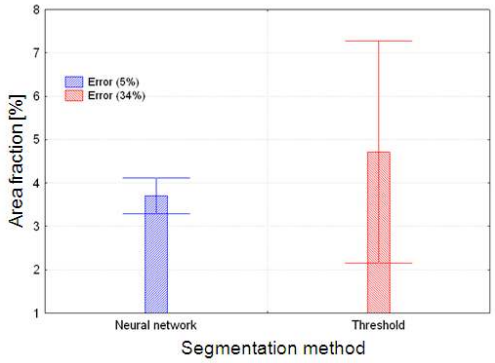

Figure 11

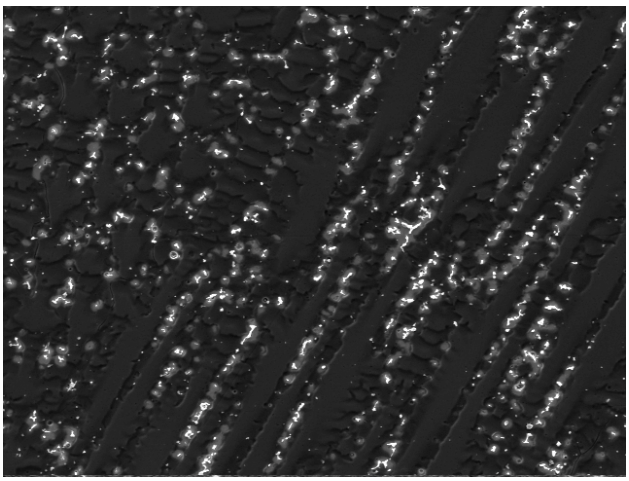

Figure 12a

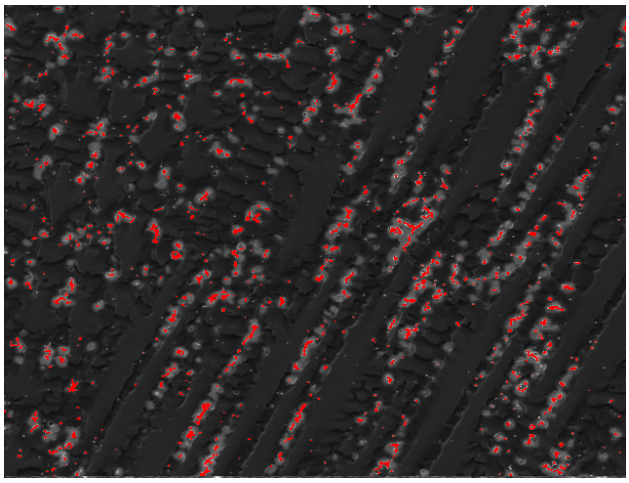

Figure 12b

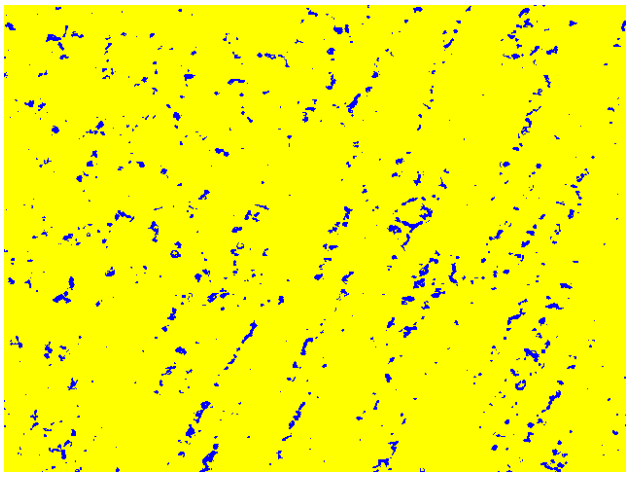

Figure 12c

TABLES

Table 1

Chemical composition (% weight)							
Ni	**Cr**	**Mo**	**Nb**	**Fe**	**Si**	**Al**	**Ti**
57.1	20.1	8.2	3.0	10.9	0.22	0.20	0.28

Table 2

Image #	New Solution (Neuronal network)		Commercial System (Threshold method)	
	Time [s]	Area [%]	Time [s]	Area [%]
1	10	1.56	22	1.27
2	9	1.54	21	1.10
3	9	1.80	25	1.70
4	10	2.15	20	1.97
5	9	2.02	18	2.30
6	10	1.84	23	2.00
7	10	2.10	24	2.20
8	10	2.84	19	2.50
9	10	2.44	22	2.30
10	9	1.84	23	2.12
11	9	4.21	20	3.80
12	8	2.26	18	3.30
13	8	2.66	17	3.20
14	8	2.63	18	3.40
15	8	3.40	22	4.00
16	9	3.37	15	3.50
17	9	2.88	17	3.30
18	9	1.53	25	1.50
19	9	2.16	19	2.60
20	9	2.34	16	2.50
Average	**9.1**	**2.74**	**20.2**	**2.53**
Standard deviation	**0.7**	**0.76**	**2.9**	**0.84**

Table 3

Image #	New Solution [%]	Specialist 1 [%]	Specialist 2 [%]	Average Specialists [%]	Difference Specialists/New Solution [%]
1	1.80	1.75	1.78	1.77	0.03
2	1.84	1.81	1.83	1.82	0.02
3	4.21	4.20	4.21	4.21	0.00
4	2.84	2.83	2.82	2.83	0.01
5	2.88	2.87	2.85	2.86	0.02
6	2.16	2.01	2.12	2.07	0.10
7	2.34	2.22	2.31	2.27	0.07
8	3.40	3.25	3.34	3.30	0.11
9	1.53	1.47	1.50	1.49	0.05
Average	**2.55**	**2.49**	**2.53**	**2.51**	**0.38**
Standard Deviation	**0.86**	**0.87**	**0.87**	**0.87**	**0.04**